Structural characterization of spray-dried microgranules by spin-echo small-angle neutron scattering

Biswas, Priyanka; Sen, Debasis; Bouwman, Wim

DOI
10.1016/j.powtec.2020.10.035

Publication date
2021

Document Version
Final published version

Published in
Powder Technology

Powder Technology 378 (2021) 680–684

Contents lists available at ScienceDirect

Powder Technology

journal homepage: www.elsevier.com/locate/powtec

Structural characterization of spray-dried microgranules by spin-echo small-angle neutron scattering

Priyanka Biswas [a,b,1], Debasis Sen [a,b,*], Wim Bouwman [c]

[a] Solid State Physics Division, Bhabha Atomic Research Centre, Mumbai 400085, India
[b] Homi Bhabha National Institute, Mumbai 400094, India
[c] Faculty of Applied Sciences, Delft University of Technology, Mekelweg 15, 2629 JB Delft, the Netherlands

ARTICLE INFO

Article history:
Received 10 July 2020
Received in revised form 8 October 2020
Accepted 9 October 2020
Available online 14 October 2020

Keywords:
Spray-drying
SESANS
SAS
Microgranules

ABSTRACT

Spray-drying is a widely used industrial technique and has shown an immense potential in the fields of nanoscience and technology. This is due to its ability to synthesize microgranules consisting of correlated nanostructures using evaporation induced assembly through bottom-up approach. Although the nature of correlation among the constituent nanoparticles and their size distribution could earlier be obtained by conventional Small-angle Scattering (SAS) technique, a statistically averaged quantitative measure of the shell thickness and hollowness of the formed granules remained a challenge. In this work, we have used Spin-echo Small-angle Neutron Scattering (SESANS) technique to characterize spray-dried nanostructured microgranules having different hollowness. It is shown that this non-destructive technique provided precise quantification of the granular sizes and hollowness by utilizing polarization property of neutrons in real space directly.

1. Introduction

Spray-drying is a well-established industrial process, used for the synthesis of powder granules from a liquid feed [1,2]. Its versatility makes it extensively useful in the food [3], pharmaceutical and chemical industries [4–14] where well-defined granules in powdered form are desired owing to the inherent advantages over their fluidic form. For example, a reduction in bulk volume makes food items suitable for transport and increase the shelf-life for all practical utilizations. In pharmaceutical industries, dried powder is often easy for medical administration through compacted granules and tablets for consumption, facilitating direct drug usage. Recent advancements in nanoscience and nanotechnology have initiated the utilization of this versatile technique into its domain as well. Since the last decade, this aerosol drying technique has proved to be an efficient bottom-up route to fabricate nanostructured microgranules [15–19] through a bottom-up self-assembly route. Such correlated nanostructured granules with well-defined shapes are obtained by rapid contact-free drying of atomized colloidal droplets. The huge enhancement of surface area by droplet atomization ensures rapid solvent evaporation, inducing directed assembly of the colloidal particles through capillarity, forming correlated nanostructured granules [15,20–28]. They retain all the characteristic properties of nanoparticles and being larger than the bare nanoparticles, they are less prone to thermal fluctuations and Brownian motion. All these traits make the granules suitable for specific applications, such as drug delivery [10], dye sorption [29], filtration [30], etc.

Colloidal droplet to powder-granular transition during the above-mentioned synthesis method is in fact, a dynamic process involving a transition from viscous to elastic phase [31]. It has been shown in recent past that the formed granules can be tuned for their morphology and hollowness by controlling the spray-drying conditions or the colloidal properties [23,32–35]. Further, the buckling of a hollow granule yields non-spherical, doughnut shapes [11,23,36–38]. The origin of such shape alteration can be due to various physico-chemical parameters, such as colloidal particle size [35], concentration [32], initial droplet size [17], viscosity [36], etc. Recently, it was demonstrated that the granular morphology shows systematic variation with the spray-drying temperature [33]. It was observed that granules exhibited a spherical to doughnut shape transformation with the increase in spray-drying temperature. Such transformation is attributed to inherent hollowness of the granules that are synthesized at higher drying temperatures. It is worth mentioning that such nanostructured microgranules are potential candidates for several technological applications. These granules are inherently porous owing to the interstices of the correlated nanoparticles constituting the granule. While such spherical granules with internal nano-porosity and hollowness

* Corresponding author at: Solid State Physics Division, Bhabha Atomic Research Centre, Mumbai 400085, India.
E-mail address: debasis@barc.gov.in (D. Sen).
[1]Present address: Polymer Engineering and Colloid Science Laboratory, Chemical Engineering Department, IIT Madras, Chennai 600036, India.

https://doi.org/10.1016/j.powtec.2020.10.035
0032-5910/

can be used as molecular sorbents [29], for drug delivery [39], water purification [40,41], encapsulation [42], etc. the doughnut-like granules with prominent central hole could be probably useful in micromachinery, such as micro-wheel, micro-bearing, base for micro dipole antenna etc. or as for granular flow modifier.

The complete structural characterization of these granules involves probing multiple length scales namely, the size of the nanoparticles (few 'nm'), interparticle distances and interaction potentials, thickness of the shell (few hundreds of 'nm') in case of the hollow granules [33,35] and the granular size as a whole (few 'μm'). A comprehensive characterization of these granules necessitates the synergic use of direct and indirect experimental techniques, such as X-ray/neutron/light scattering [43] and electron microscopy [44]. Scanning Electron Microscopy (SEM) provides the overall external morphology of the granules [45]. Typical hydrodynamic lengths of the granules are obtained by Dynamic Light Scattering (DLS) technique [46]. However, both DLS and SEM are non-intrusive techniques; hence fall short in quantifying statistically-averaged information about the various length scales and structure of the granules. Small-Angle Scattering (SAS) picks up on these drawbacks by providing a realistic quantification of the size, internal structure and nanoparticle correlation in the hierarchical granules. Thus, imaging or DLS results should be corroborated with the small-angle scattering (SAS) techniques to provide a holistic view of the granular structure [47–49]. A conventional SAS technique measures the variation of neutron/X-ray scattering intensity ($I(q)$) as a function of wave vector transfer (q) in the small q regime. $I(q)$ is the Fourier transform [50] of the auto-correlation function ($\gamma(r)$) of the density distribution ($\rho(r)$). Thus, size information (in real space) needs to be extracted from the scattering profile which is in the Fourier space. Estimation of overall granular size, shell thickness and shape demand accessibility of extremely small q regime. However, the finite angular divergence of probing radiation puts a constraint on the minimum q accessible in a SAS experiment, reaching up to order of ~100 nm, or up to 1 μm in case of measurements by Ultra SANS (USANS). Multiple scattering is also a major problem in these cases. In this regard, an alternative way of performing SAS experiments using the spin-echo principle provides information even up to tens of microns in real space.

Spin-echo Small-Angle Neutron Scattering (SESANS) utilizes the polarizing property of neutrons for real dimension determination [51–53]. This technique proves to be efficient in providing a statistically-averaged quantification of the overall sizes as well as the shell thicknesses. It has a unique advantage as it allows investigations even of the order of 10 μm in the real space without compromising much of the resolution. In this technique, the depolarization of a polarized neutron beam is measured as a function of the "spin-echo length" Z, which is a real space parameter [54]. SESANS approach relates the polarization $P(Z)$ of the neutron beam to the projection $G(Z)$ of the auto-correlation function ($\gamma(r)$) of the density distribution ($\rho(r)$) of the sample [54,55]. $P(Z)$ is measured as a function of the real-space distance over which correlations are measured in the sample or the spin-echo length (Z). Rekveldt *el al.* (2005) [53] and Bouwman et al. (2004) [51] established the technical details of instrumentation, theoretical background required and cited applications of SESANS. Reproducibility of $G(Z)$ profiles from $I(q)$ and vice-versa was also established through Hankel and inverse Hankel transformations, respectively [54].

In this paper, we probe spray-dried nanostructured microgranules using SESANS to estimate the granular size and the shell thickness. The quantification of the average granule size and shell thickness which was earlier elusive [33], has now been obtained using SESANS. The main motivation of this work is to establish a bridge between SESANS and conventional complementary characterization techniques, thus demonstrating SESANS as an efficient tool for quantitative characterization of nanostructured microgranules, along with complementary microscopy or spectroscopic tools.

2. Experimental methods

The synthesis process of the granules is elaborated in Biswas et al. [33] In short, 2% by weight aqueous nano-silica dispersion was used as the spray drying feed. Spray dryer Labultima LU 228 was used for the purpose. Aqueous dispersion was fed into an air-compressed atomizer nozzle the rate of 2 mL/min. Droplets with an average size of ~10 μm were obtained. Hot air causes these droplets to dry, resulting in dry powder being collected at the cyclone separator. The aspirator rate was kept fixed at 50 m^3/h and atomization pressure at 2 kg/cm^2. Only the drying temperature was adjusted to 110 °C, 130 °C, 160 °C and 180 °C and powder was obtained in each case. For reference, the powder samples will be referred to as P-110, P-130, P-160 and P-180 corresponding to each of the synthesis temperatures.

DLS experiments were performed using HORIBA DLS SZ100 Japan on diluted aqueous dispersion of the granules. The morphology of the assembled granules was examined using field emission scanning-electron-microscope (FE-SEM), Carl Zeiss Gemini 300SEM, Germany, FE-SEM model. SESANS measurements were carried out at the reactor at TU, Delft, Netherlands. The principles of the SESANS technique is elaborated in Rekveldt et al. [53]

3. Results and discussions

It is perceived from the FESEM micrographs (Fig. 1 and Fig. SI 1) in the Supplementary Information) that P-110 and P-130 granules are predominantly spherical, whereas P-160 and P-180 are larger and doughnut-shaped.

Inset on P-180 in Fig. 1 shows a cracked granule, where the shell clearly visible. An overall picture (Fig. SI 1) depicts that the granules are polydisperse in shape and sizes. This is because the spray-drying process, although tuneable to a large extent, has some limitations regarding the initial drop size polydispersity. The origin for such diversity has been demonstrated earlier in Biswas et al. and will also be summarised later in the manuscript.

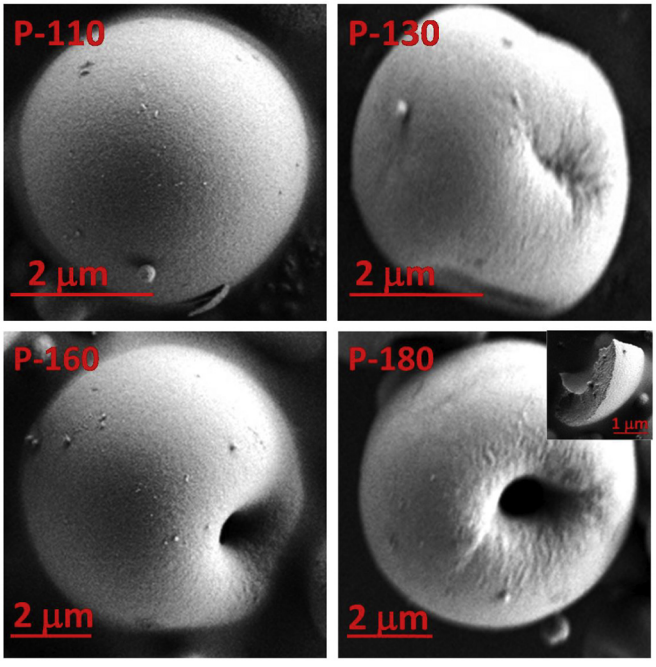

Fig. 1. FESEM micrographs of the granules depicting the shape diversity at different drying temperatures. The inset of P-180 shows the hollowness of the granules.

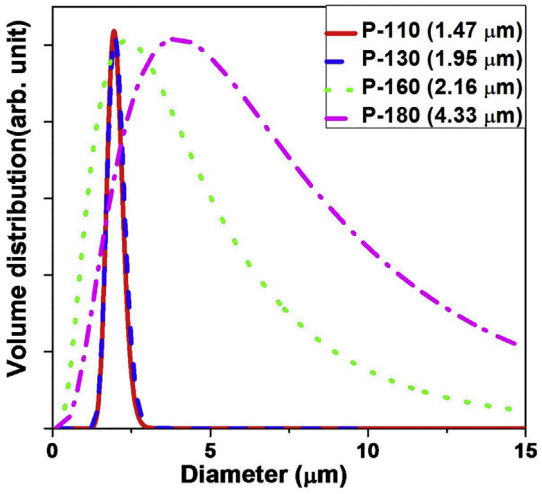

Fig. 2. Granular diameter distribution as obtained from DLS [33].

Results of DLS measurement, provided on Fig. 2, graphically quantifies the hydrodynamic sizes of the granules. The hydrodynamic sizes for each have been provided in the notation panel.

It is to be noted here that the size quantification obtained from DLS are not the actual granular sizes. DLS assumes a consolidated spherical shape of the granule from which the resultant hydrodynamic radii/diameters are obtained. However, for hollow granules the solid sphere assumption is erroneous. Nonetheless, DLS do provide the polydispersity trend of the granular size. Hence, corroborating DLS results with microscopy or small-angle scattering is imperative. Details on comparison of DLS results with FESEM image analysis was discussed in Biswas et al. [33] In the present work, we quantify the average granular sizes along with the shell thickness with the help of SESANS, which was not earlier possible with the aforementioned techniques.

Before going into the details of the SESANS technique, it is important to understand the origin of the granular shape and size variation with drying temperature [33]. During drying of a droplet the nanoparticles undergo a diffusive motion. Drying temperature plays a significant role in directing the motion of the nanoparticles. Often, the drying rate at the evaporation front or the air-liquid interface is quick enough to interlock the particles at the droplet edge into a shell, before it could diffuse back to the centre. This shell is porous due to the interstices formed due to the jamming of the nanoparticles. With time, evaporation of trapped water progresses through this porous shell. During such a transport of solvent, pressure imbalance develops across the shell, which ultimately causes it to buckle, giving a distorted spherical or doughnut-shaped granule, which is precisely the case at higher drying temperatures. At lower dying temperatures, the assembly is much more compact as the nanoparticles find enough time to rearrange, allowing the shell to thicken considerably, leading to a more isotropic granular shape. As mentioned earlier, size determination from DLS and FESEM can only provide the polydispersity trend and not the size quantification. For a more dependable statistically-averaged quantification, resorting to scattering techniques is crucial.

Over the years, SAS has been established as an efficient non-destructive tool for characterization of mesoscopic length scales. Information about structure and correlation is obtained in reciprocal space, as a function of wave vector transfer, '*q*'. For hierarchically structured granules, such as in the present case, accessibility of a wide *q*-range is required. Often, due to instrumental constraints of one, multiple SAS instruments are used to probe all the relevant length scales. In the present case, the two important length scales are the micrometric granular size and the nanoparticle size. Moreover, in the case of hollow granules, the thickness of the shell also holds significance.

In our earlier work, we have reported results of SAXS and SANS analysis for the granules in details. SAXS reveals the nanoparticle size to be ~14 nm. The packing fraction was found to be ~0.7 which is slightly more than random jamming packing (~0.64) in all of the cases. [33] A sticky hard sphere type interactive potential exists between the jammed particles [56]. The SAXS profiles are provided in Fig. SI 2 where a distinct correlation peak is observed at the same *q*-position for all the cases, denoting that average centre-to-centre nanoparticles distance of ~25 nm. Further, Biswas et al. [33] ruled out any possibility of ramified fractal-like aggregation in large-sized granules from the fitting of SANS profiles, denoting that the nanoparticles are uniformly jammed, and therefore the reason for the formation of large-sized granules is creation of internal hollowness. However, this hollowness or the granule size could not be quantified by conventional SAS techniques due to instrumental constraints of achieving extremely low scattering angle regime because of direct beam effect. This justifies the use of a relatively newer version of the SAS technique using spin-echo principle, known as Spin Echo Small-Angle Neutron Scattering (SESANS) [51–55,57–60].

In SESANS principle, a sample of thickness '*t*', having a differential scattering cross-section of $\frac{d\Sigma(\vec{q})}{d\Omega}$ is assumed, on which a neutron beam of cross-section '*S*', wavelength 'λ' is incident. It is known that neutrons undergo Larmor precession in a magnetic field. The scattering event will cause a change in this precession depending on the angle at which the neutrons are scattered [54]. Initially polarized (P_0) neutron beam becomes depolarized due to elastic scattering by the sample. The depolarization plots for each of the powder granules are given in Fig. 3.

The total detected polarization P_d of the neutron beam is a function of the spin-echo length *Z* given by the expression $\frac{P_d(Z)}{P_0} = e^{[G(Z)-G(0)]} = e^{G(0)[G_0(Z)-1]}$ where $G_0(Z)$ is the normalized $G(Z)$ given by $\frac{G(Z)}{G(0)}$ and $G(Z)$ has the form,

$$G(Z) = \frac{\lambda^2 t}{4\pi^2} \int_{-\infty}^{\infty} dq_y \int_{-\infty}^{\infty} dq_z \frac{d\Sigma(\vec{q})}{d\Omega} \cos(q_z Z)$$

and $\vec{q} = (0, q_y, q_z)$, the spin-echo length is given by $Z = c\lambda^2 BL \cot\frac{\theta_0}{2\pi}$ where the neutron wavelength λ is 0.21 nm and inclination angle $\theta_0$is 5.5°. The spin-echo length, *Z* can be tuned by varying the magnetic field *B* and distance *L* (between the sample and the last magnet). *Z* is physically the length which the correlations are probed [55,57–60]. More details of the technique have been elucidated in the works of Andersson et al. [60] *G*(*Z*)-*G*(0) profiles were obtained using, $G(Z) = \frac{\ln(P(Z))}{s} + 1$,

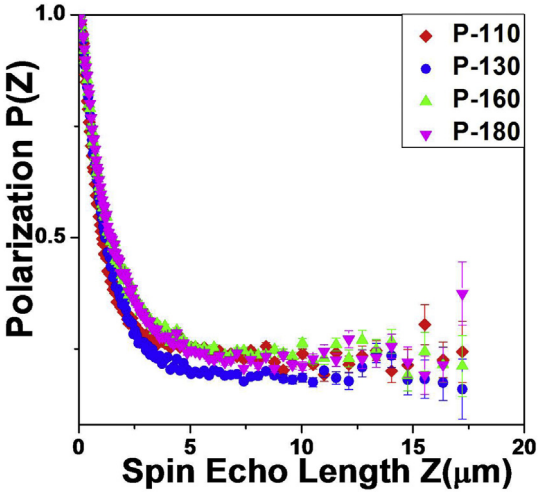

Fig. 3. Depolarization plots obtained from SESANS measurements.

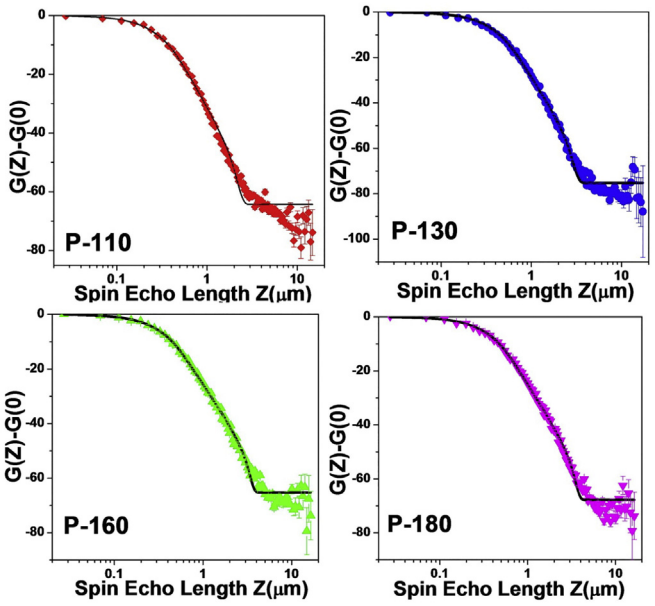

Fig. 4. Normalized $G(Z)$-$G(0)$ profiles obtained from depolarization plots. The solid line shows the fit of the model.

Table 1
Fitting parameters from analysis of the SESANS profiles.

Granules	Outer Radius (μm)	Inner radius (μm)	Inner hollow space volume (μm^3)
P-110	1.44 ± 0.006	0.86 ± 0.008	3.05
P-130	1.91 ± 0.010	1.14 ± 0.011	5.60
P-160	2.10 ± 0.011	1.44 ± 0.013	11.5
P-180	2.20 ± 0.013	1.47 ± 0.014	14.13

where '*s*' is the total cross-section of the sample and $P(Z)$ is the polarization. The fit of $G(Z)$-$G(0)$, is shown in Fig. 4 where $G(Z)$ have been fitted using SASFIT software [61] by assuming a monodisperse spherical shell model. The fitting parameters are tabulated in Table 1.

The granular sizes as well as the inner hollow space volume were found to increase gradually for granules synthesized at higher drying temperatures. An average shell thickness of ~700 nm was obtained from the SESANS profiles as well. Here it should be noted that the use of a polydisperse model with hollow geometry requires several parameters which makes the estimation of these parameters through nonlinear least-square highly unreliable. First of all, considering polydispersity in fitting for such hollow geometry is difficult because both inner and outer granular radius polydispersity has to be factored in. However, for any practical purpose, considering such multi-polydispersity is unfeasible as far as the SESANS analysisis concerned. Therefore we report the statistically-averaged value of granular sizes and shell thicknesses. We would also point out that considering a strictly monodisperse model is unrealistic as it demands several idealistic experimental conditions, such as monodisperse droplet generator, non-coalescence of the droplets, very slow drying rate, etc. In such theoretical cases, the formation of shell does not occur and compacted spherical granules are formed. Another important observation was that in the case of P-110, the fit of the $G(Z)$ profile at higher Z is slightly compromised. This is probably due to agglomeration of a large number of small-sized granules due to electrostatic charging. This problem does not exist for larger granules (P-180). A proper fix would be to synthesize a more uniformly sized batch of the granules by ensuring droplet size monodispersity.

4. Conclusions

It has been established that Spin-Echo Small-angle Neutron Scattering (SESANS) is an effective, non-destructive technique for the structural quantification of hollow spray-dried micro-granules. Granules were synthesized by spray-drying of dilute nano-silica colloidal dispersion at different drying temperatures. Structural characterization of the obtained granules by electron microscopy and dynamic light scattering showed that the granules synthesized at higher spray-drying temperatures are larger than those synthesized at lower drying temperatures along with distinct shape differences. At lower drying temperatures, the granules are spherical whereas at higher temperatures doughnut-shaped granules are obtained. SESANS quantified the average granular size and shell thicknesses which were not previously possible with conventional small-angle scattering experiments. It was found that the granules are hollow with an average shell thickness of 700 nm and internal core volume varying from ~3 μm^3 for spherical granules at low drying temperatures, up to ~14 μm^3 for doughnut-shaped granules. In future, we plan to carry out spray-drying with an ultrasonic nebulizer instead of the compressed-air atomizer. This is expected to provide a narrower droplet size distribution vis-a-vis the assembled granules with less size polydispersity and more uniformity in shell thicknesses.

Declaration of Competing Interest

Authors declare no conflict of interest.

Acknowledgements

The authors would like to thank the developers of SASFIT software, Dr.Joachim Kohlbrecher and Dr.Ingo Bressler, Paul Scherrer Institut (PSI), Switzerland.

Appendix A. Supplementary data

Supplementary data to this article can be found online at https://doi.org/10.1016/j.powtec.2020.10.035.

References

[1] K. Masters, Spray Drying Handbook, 5th ed. Longman Scientific & Technical, Harlow, Essex, U.K., 1991
[2] C. Anandharamakrishnan, S. Padma Ishwarya, Spray Drying Techniques for Food Ingredient Encapsulation, 1st ed. John Wiley & Sons, 2015.
[3] A. Gharsallaoui, et al., Applications of spray-drying in microencapsulation of food ingredients: an overview, Food Res. Int. 40 (2007) 1107–1121.
[4] M. Ameri, Y.F. Maa, Spray drying of biopharmaceuticals: stability and process considerations, Dry. Technol. 24 (2006) 763–768.
[5] R. Vehring, Pharmaceutical particle engineering via spray drying, Pharm. Res. 25 (2008) 999–1022.
[6] M. Jain, et al., Spray drying in pharmaceutical industry: a review, Res. J. Pharm. Dosage Forms Technol. 4 (2012) 74–79.
[7] J. Patil, Spray-drying: an emerging technique for pharmaceutical product development, Aust. J. Pharm. 4 (2016) 2.
[8] P.B. Fourie, et al., Spray drying TB vaccines for pulmonary administration, Expert. Opin. Biol. Ther. 8 (2008) 857–863.
[9] D. McAdams, D. Chen, D. Kristensen, Spray drying and vaccine stabilization, Expert Rev. Vaccines (10) (2012) 1211–1219.
[10] L. Peltonen, et al., Electrospraying, spray drying and related techniques for production and formulation of drug nanoparticles, Expert Opin. Drug Deliv. 7 (6) (2010) 705–719.
[11] D. Sen, et al., Use of small-angle neutron scattering to investigate modifications of internal structure in self-assembled grains of nanoparticles synthesized by spray drying, J. Colloid Interface Sci. 347 (1) (2010) 25–30.
[12] D. Sen, et al., Slow drying of a spray of nanoparticles dispersion. In situ SAXS investigation, Langmuir 23 (8) (2007) 4296–4302.
[13] A. Thill, O. Spalla, Influence of templating latex on spray dried nanocomposite powders studied by small angle scattering, J. Colloid Interface Sci. 291 (2) (2005) 477–488.
[14] K. Waldron, et al., Formation of monodisperse mesoporous silica microparticles via spray-drying, J. Colloid Interface Sci. 418 (2014) 225–233.
[15] S.Y. Lee, et al., Formation of highly ordered nanostructures by dryingmicrometer colloidal droplets, ACS Nano 4 (2010) 4717–4724.

[16] C. Boissiere, et al., Aerosol route to functional nanostructured inorganic and hybrid porous materials, Adv. Mater. 23 (5) (2011) 599–623.
[17] F. Iskandar, L. Gradon, K. Okuyama, Control of the morphology of nanostructured particles prepared by the spray drying of a nanoparticle sol, J. Colloid Interface Sci. 265 (2) (2003) 296–303.
[18] F. Iskandar, et al., Functional nanostructured silica powders derived from colloidal suspensions by sol spraying, J. Nanopart. Res. 3 (4) (2001) 263–270.
[19] C.J. Brinker, et al., Evaporation-induced self-assembly: nanostructures made easy, Adv. Mater. 11 (7) (1999) 579–585.
[20] A. Khan, et al., Design and performance of a laboratory spray dryer to realize evaporation-induced self-assembly of nanoparticles, Dry. Technol. 30 (6) (2012) 679–686.
[21] W. Liu, et al., Facile spray-drying assembly of uniform microencapsulates with tunable core-shell structures and controlled release properties, Langmuir 27 (21) (2011) 12910–12915.
[22] D. Sen, et al., Evaporation driven self-assembly of a colloidal dispersion during spray drying: volume fraction dependent morphological transition, Langmuir 25 (12) (2009) 6690–6695.
[23] D. Sen, et al., Buckling-driven morphological transformation of droplets of a mixed colloidal suspension during evaporation-induced self-assembly by spray drying, Eur. Phys. J. E. 31 (4) (2010) 393–402.
[24] D. Sen, O. Spalla, A. Thill, Nanocomposite powders by evaporation driven self assembly during spray drying: some new insights on the structure modifications, Solid State Phenom. 128 (2007) 73–80.
[25] J. Bahadur, et al., Evaporation driven self-assembly of nanoparticles during spray drying: volume fraction dependent packing, Int. J. Nanosci. 10 (4–5) (2011) 995–999.
[26] S. Lyonnard, et al., Role of interparticle potential in controlling the morphology of spray-dried powders from aqueous nanoparticle sols, Langmuir 18 (26) (2002) 10386–10397.
[27] J.S. Melo, et al., Spray drying as a novel technique for obtaining microbial imprinted microspheres and its application in filtration, Soft Matter 9 (2013) 805.
[28] K. Waldron, et al., Formation of uniform large SBA-15 microspheres via spray drying, J. Mater. Chem. A 2 (2014) 19500–19508.
[29] P. Biswas, et al., Porous microcapsules comprised inter-locked nano-particles by evaporation-induced assembly: evaluation of dye sorption, Colloids Surf. A Physicochem. Eng. Asp. 520 (2017) 279–288.
[30] A. Das, et al., Formation of nano-structured core–shell micro-granules by evaporation induced assembly, RSC Adv. 5 (2015) 85052–85060.
[31] L. Pauchard, C. Allain, Buckling instability induced by polymer solution drying, Europhys. Lett. 62 (2003) 897–903.
[32] J. Bahadur, et al., Evaporation-induced self assembly of nanoparticles in non-buckling regime: volume fraction dependent packing, J. Colloid Interface Sci. 351 (2) (2010) 357–364.
[33] P. Biswas, et al., Temperature mediated morphological transition during drying of spray colloidal droplets, Langmuir 32 (10) (2016) 2464–2473.
[34] D. Sen, et al., Formation of hollow spherical and doughnut microcapsules by evaporation induced self-assembly of nanoparticles: effects of particle size and polydispersity, Soft Matter 8 (2012) 10036–10044.
[35] J. Bahadur, et al., Origin of buckling phenomenon during drying of micrometer-sized colloidal droplets, Langmuir 27 (2011) 8404–8414.
[36] D. Sen, et al., Nanocomposite silica surfactant microcapsules by evaporation induced self assembly: tuning the morphological buckling by modifying viscosity and surface charge, Soft Matter 8 (6) (2012) 1955–1963.
[37] D. Sen, et al., Arrest of morphological transformation during evaporation-induced self-assembly of mixed colloids in micrometric droplets by charge tuning, Soft Matter 7 (11) (2011) 5423–5429.
[38] D. Sen, et al., Temperature effects on the composition and microstructure of spray-dried nanocomposite powders, Langmuir 22 (8) (2006) 3798–3806.
[39] S.S. Guterres, et al., Spray-drying technique to prepare innovative nanoparticulated formulations for drug administration: a brief overview, Braz. J. Phys. 39 (2009) 205–209.
[40] D. Sen, et al., Novel polysulfone–spray-dried silica composite membrane for water purification: preparation, characterization and performance evaluation, Sep. Purif. Technol. 123 (2014) 79–86.
[41] J.S. Melo, et al., Spray drying as a novel technique for obtainingmicrobial imprinted microspheres and its application infiltration, Soft Matter 9 (2013) 805–810.
[42] A. Das, et al., Formation of nano-structured core–shell micro-granules by evaporation induced assembly, RSC Adv. 5 (2015) 85052–85060.
[43] T. Zemb, P. Lindner, Neutron, X-rays and Light. Scattering Methods Applied to Soft Condensed Matter, Elsevier, Amsterdam, 2002.
[44] U. Valdre, Electron Microscopy in Material Science, Academic Press, New York, 1971.
[45] W. Zhou, Z.L. Wang, Scanning Microscopy for Nanotechnology, Springer, New York, 2006.
[46] W. Burchard, Static and Dynamic Light Scattering from Branched Polymers and Biopolymers, Springer, Berlin, 1983.
[47] L.A. Feigin, D.I. Svergun, Structural Analysis by Small Angle X-Ray and Neutron Scattering, Plenum Press, New York, 1987.
[48] O. Glatter, O. Kratky, Small Angle X-ray Scattering, Academic Press, New York, 1982.
[49] A. Guinier, et al., Small Angle Scattering of X-rays, Wiley, New York, 1955.
[50] R. Bracewell, The Fourier Transform and Its Applications, 3rd ed. McGraw-Hill Book Co., New York, 1999.
[51] W.G. Bouwman, et al., SESANS studies of colloid phase transitions, dairy products and polymer fibres, Physica B 350 (2004) 140–146.
[52] T. Krouglov, et al., Structural transitions of hard-sphere colloids studied by spin-echo small-angle neutron scattering, J. Appl. Crystallogr. 36 (2003) 1417–1423.
[53] M. Rekveldt, et al., Spin-echo small angle neutron scattering in Delft, Rev. Sci. Instrum. 76 (2005) 33901–33909.
[54] M.T. Rekveldt, et al., Elastic neutron scattering measurements using larmor precession of polarised neutrons, in: C.P.F. Mezei, T. Gutberlet (Eds.), Neutron Spin Echo Spectroscopy, Lecture Notes in Physics, Springer, Berlin, 2003.
[55] F. Mezei, Neutron Spin-Echo. Lecture Notes in Physics, ed. F. Mezei. 128, Springer, Berlin, 1980.
[56] R.J. Baxter, Percus–Yevick Equation for hard spheres with surface adhesion, J. Chem. Phys. 49 (1968) 2770–2774.
[57] R. Gähler, et al., Space-time description of neutron spin echo spectrometry, Physica B 229 (1996) 1–100.
[58] J. Zhao, Concepts in spin echo small-angle neutron scattering, J. Appl. Crystallogr. 34 (2001) 639–645.
[59] R. Gahler, et al., Space-time approach to scattering from many-body systems, Phys. Rev. A 58 (1998) 280–295.
[60] R. Andersson, et al., Analysis of spin-echo small-angle neutron scattering measurements, J. Appl. Crystallogr. 41 (2008) 868–885.
[61] I. Breßler, J. Kohlbrecher, A.F. Thünemann, SASfit: a tool for small-angle scattering data analysis using a library of analytical expressions, J. Appl. Crystallogr. 48 (2015) 1587–1598.